

**Supporting information for**

# **Laser printing of 2D transition metal dichalcogenide diffractive optical elements**

**Arina O. Kalganova<sup>1, \*</sup>, Aleksandr V. Averchenko<sup>1</sup>, Igor A. Salimon<sup>1</sup>, Omar A. Abbas<sup>2</sup>, Ekaterina D. Grayfer<sup>1</sup>, Pavlos G. Lagoudakis<sup>1</sup>, and Sakellaris Mailis<sup>1, \*</sup>**

<sup>1</sup> Center for Photonic Science and Engineering (CPhSE), Skolkovo Institute of Science and Technology, 3 Nobel Street, 143026, Moscow, Russian Federation

<sup>2</sup> College of Engineering, Al-Nahrain University, Baghdad, 10072, Iraq

[\\*Arina.Kalganova@skoltech.ru](mailto:Arina.Kalganova@skoltech.ru)

[\\*S.Mailis@skoltech.ru](mailto:S.Mailis@skoltech.ru)

## Thickness analysis of laser-irradiated precursors

The comparison of thickness and composition of pre-patterned and synthesized tracks was done with Raman spectroscopy and AFM measurements.

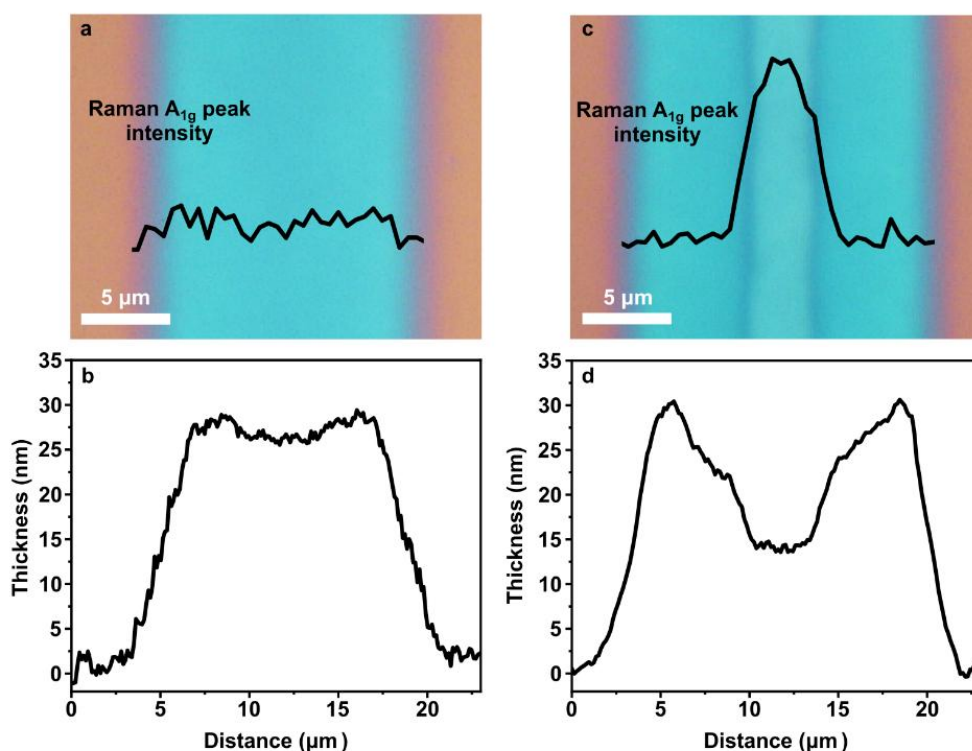


**Fig. S1.** Optical images and corresponding AFM profiles of tracks produced from  $(\text{NH}_4)_2\text{MoS}_4$  precursor by single-beam laser scanning. (a) Optical image of amorphous track produced using a laser peak intensity of  $0.5 \text{ MW cm}^{-2}$  and (b) corresponding AFM profile made across the track. (c) Optical image of a track produced using a  $0.7 \text{ MW cm}^{-2}$  peak intensity of laser beam. The superimposed graphs to the optical microscopy images a and b correspond to the amplitude of the  $A_{1g}$  Raman peak, across the track. The  $A_{1g}$  Raman peak appears only in the central region of the track shown in (c) corresponding to synthesized polycrystalline  $\text{MoS}_2$ , while it is absent in the side lobes, which consist of amorphous  $\text{MoS}_3/\text{MoS}_2$ . (d) AFM profile of the track, which have been produced using peak intensity of  $0.7 \text{ MW cm}^{-2}$ , showing shrinkage in the central area that corresponds to laser-synthesized  $\text{MoS}_2$  (thickness  $\sim 14 \text{ nm}$ ) and thicker amorphous side lobes (thickness  $\sim 30 \text{ nm}$ ). The AFM scans reveal that the thickness of the pre-patterned precursor (b) matches the thickness of side lobes in the case of direct laser synthesis (d).

## The TMDCs grating production process

Preparation of TMDCs diffractive structures was done implying interference patterning approach with two-step synthesis process.

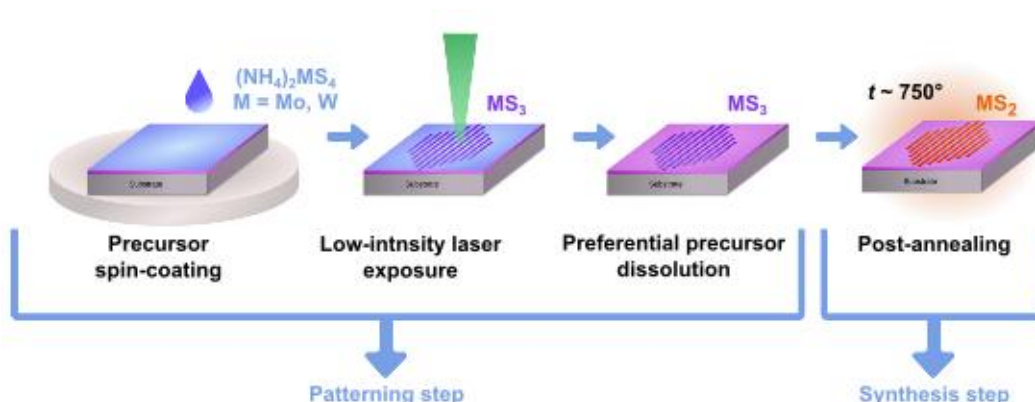


**Fig. S2.** Schematic representation of the two-step production of TMDC gratings from the single-source thiosalt precursor  $(\text{NH}_4)_2\text{MS}_4$  ( $M = \text{Mo}, \text{W}$ ). The precursor film, which was produced according to the process mentioned in the Experimental section, is irradiated with low intensity visible or UV C.W. laser radiation inducing thermal decomposition of the precursor (in ambient conditions) and producing locally amorphous  $\text{MoS}_2/\text{MoS}_3$ . Then, the non-irradiated regions dissolve away in NMP solvent revealing the structured amorphous material which adheres to the substrate. As the second step, the micro/nano-structured amorphous material is converted to TMDC by high temperature furnace annealing or by high intensity laser annealing.

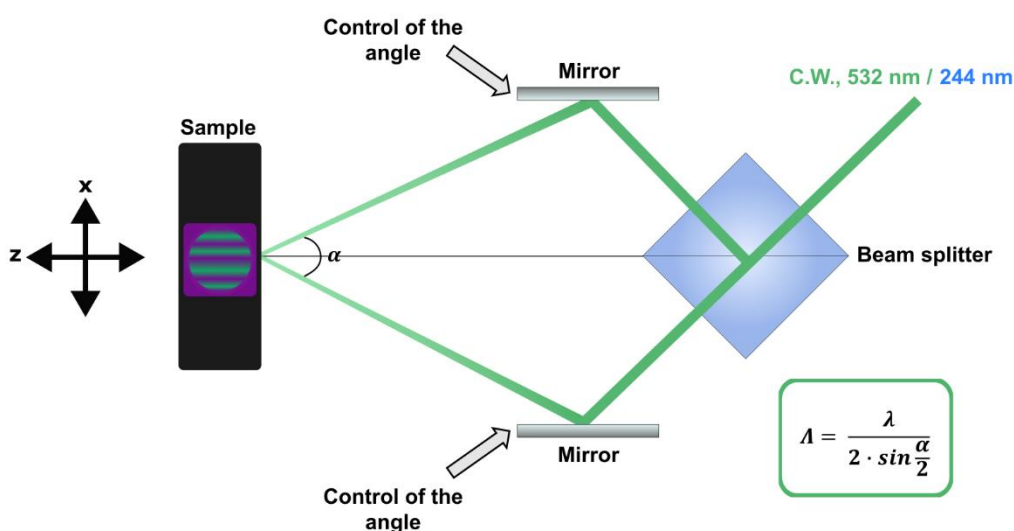


**Fig. S3.** Schematic of the experimental setup used for direct laser interference patterning of TMDC materials. The C.W. laser source divided into two beams using a silica grating (phase mask optimized for 244 nm) as a beam splitter for the 244 nm laser beam and a non-polarizing cube beam splitter for the 532 nm beam. Two separate beams overlapped onto the sample surface at an angle  $\alpha$ , thus determining the period of the interference pattern and consequently the period of the resulting grating. The spot size was adjusted by using a spherical lens placed before the beam splitter.

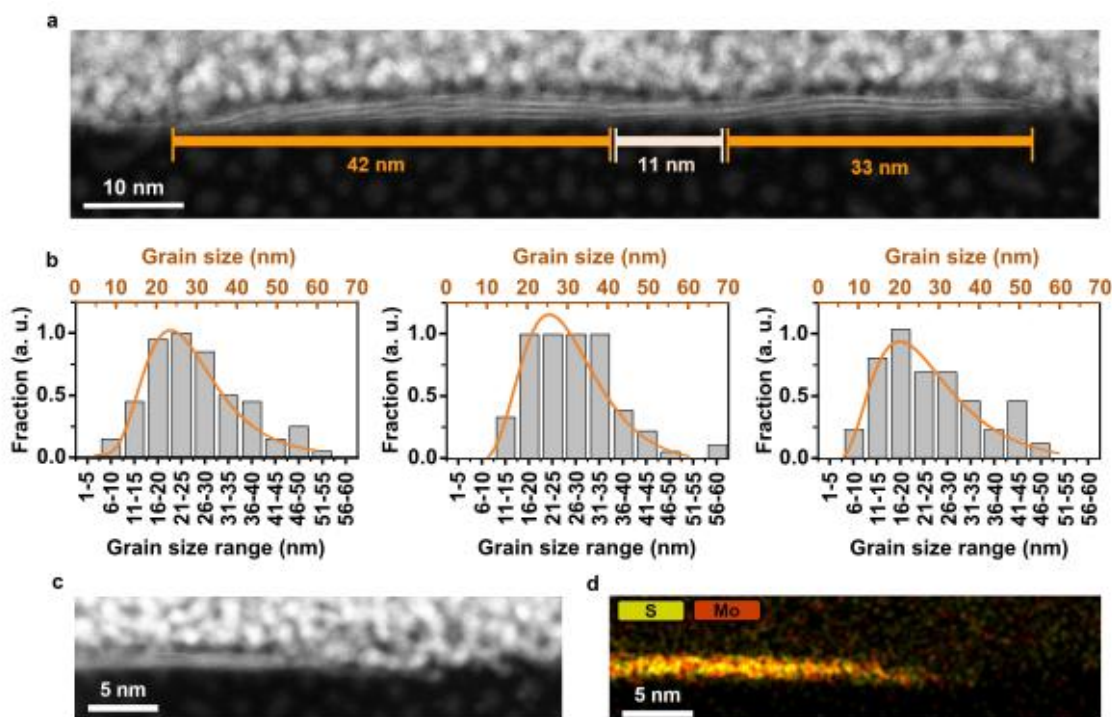


**Fig. S4.** (a) TEM image of an individual MoS<sub>2</sub> fringe from the grating with a period of 150 nm. The markers correspond to the grain length inside the fringe cross section. (b) Histograms of the grain size distribution within the MoS<sub>2</sub> gratings with periods of 620 nm, 360 nm and 150 nm. The solid orange line superimposed on the histograms corresponds to a lognormal distribution. (c) STEM image and (d) EDS map acquired on the crest/trough boundary of a MoS<sub>2</sub> fringe/nanoribbon of a grating with a period of 150 nm. The red and yellow colors correspond to the molybdenum and sulfur atoms, respectively.

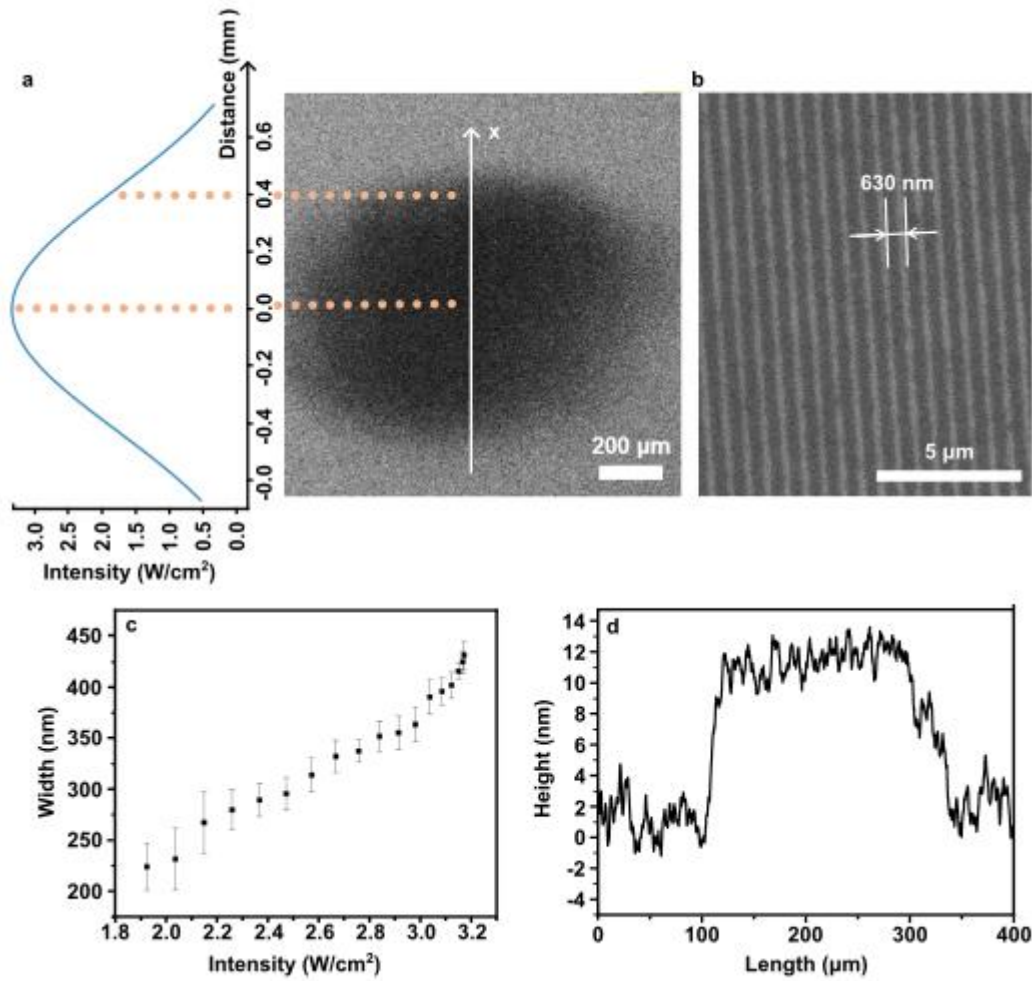


**Fig. S5.** (a) Low resolution SEM image of imprinted spot containing a MoS<sub>2</sub> grating with a period of 630 nm (right) and corresponding intensity envelope distribution of the interfering beams across the irradiated spot (left). (b) Close up SEM image of the MoS<sub>2</sub> grating shown in (a). The dark areas correspond to MoS<sub>2</sub> (c) Plot of the nanoribbon width as a function of the irradiating intensity. The mean nanoribbon width value was calculated by averaging the widths of 5 adjacent nanoribbons for each intensity value. (d) Profile envelope of the spot after development and before annealing, showing uniform thickness across the pattern.

## Intensity distribution calculation details

The intensity distribution across the spot diameter was determined as an interference of Gaussian laser beams. According to Gaussian beam theory, the peak intensity can be determined from laser beam power (P) and width (w) as:

$$I_0 = \frac{2P}{\pi w^2}$$

In this case, the intensity distribution for a single Gaussian beam can be defined as:

$$I(x, y) = I_0 \cdot \exp\left(-\frac{2(x^2 + y^2)}{w^2}\right)$$

The intensity distribution for an two-beam interference can be calculated as:

$$I_{int}(x, y) = 2I(x, y) + 2I(x, y) \cdot \cos(\varphi x)$$

$$\varphi = \frac{4\pi \sin \alpha \sin \frac{\alpha}{2}}{\lambda}$$

The modeling was performed applying the Python modeling with NumPy and Matplotlib libraries for laser power (P) of 9 mW and beam width (w) of 0.45 mm.

## Ellipsometry analysis

Experimentally measured ellipsometry spectra were analyzed by SpectraRay/4 software. The Fresnel multilayer model was utilized to fit experimentally measured spectra. The sample was taken as 10 nm MoS<sub>2</sub> on top of 300 nm SiO<sub>2</sub> on Si substrate (considered infinite). To fit permittivity, we used three Tauc-Lorentz (TL) oscillators model which considered  $\varepsilon_2$  as:

$$\varepsilon_2 = \begin{cases} \frac{1}{E} \cdot \frac{AE_0C(E - E_g)^2}{(E^2 - E_0^2)^2 + C^2E^2} & \text{for } E > E_g \\ 0 & \text{for } E < E_g \end{cases}$$

Here,  $E$  is related to the photon energy,  $A$  is the strength of the oscillator,  $E_0$  is the resonance frequency and  $C$  is the broadening of the oscillator. The  $\varepsilon_1$  is obtained from  $\varepsilon_2$  expression in the model using Kramers-Kronig integration. The  $\varepsilon_1$  was found from  $\varepsilon_2$  by Kramers-Kronig integration. The parameters chosen for theoretical model are presented in Table S1.

**Table S1.** The parameters of Tauc-Lorentz oscillators for ellipsometry modelling considering  $\varepsilon_1^\infty$  as 1.

Oscillator	$A$	$C$	$E_0$ (eV)	$E_g$ (eV)
#1	670.848	134.012	1.876	0.881
#2	273.403	4.809	2.102	1.855
#3	60.965	0.521	2.705	2.056